International Journal of Multiphase Flow 169 (2023) 104609

Contents lists available at ScienceDirect

International Journal of Multiphase Flow

journal homepage: www.elsevier.com/locate/ijmulflow

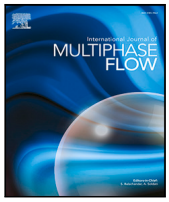

Assessment of the parcel model in evaporating turbulent diluted sprays within a Large-Eddy-Simulation approach

Jietuo Wang [a], Federico Dalla Barba [b,*]

[a] Department of Mechanics Mathematics and Management, Polytechnic University of Bari, Bari, BA 70125, Italy
[b] Department of Industrial Engineering, University of Padova, Padova, PD 35131, Italy

ARTICLE INFO

Keywords:
Spray dynamics
Lagrangian modelling
Parcel model
Droplet evaporation
LES

ABSTRACT

The parcel concept has been exploited in the Eulerian–Lagrangian framework to alleviate the computational cost of tracking an enormous number of particles/droplets in the perspective of dispersed two-phase flows. In this work, with fully systematic analysis, we present a numerical investigation of the reliability of this parcel approach in turbulent flows bearing evaporating droplets. To fulfil this task, we address Large-eddy Simulations (LESs) of a turbulent diluted acetone jet-spray in conjunction with two filtering widths and various numbers of parcels, in which the latter is achieved by reducing the ensemble of all physical droplets with a coarsening factor varying from $\mathcal{O}(1)$ to $\mathcal{O}(1000)$, i.e. parcel ratio (PR). By comparing different realizations of parcel in LESs against that with $PR = 1$, as well as a fully resolved Direct Numerical Simulation (DNS), our numerical results demonstrate the robustness of the parcel concept only when the ratio between the computational and physical droplets is carefully implemented, depending on the grid spacing. In particular, a significant underestimation of the evaporation process is anticipatable if the parcel ratio exceeds a specific threshold which is much larger in the case of a coarse mesh than a fine one. We propose that the appropriate parcel ratio should be of the order of the filtering width and the dissipative length ratio, thus of the same order as the coarsening factor of the Eulerian mesh spacing with respect to the reference DNS.

1. Introduction

Dispersed two-phase flows are frequently found in daily life and numerous natural and industrial processes, such as droplets transmission in respiratory events, sediment transport in rivers, bubbles uprising in chemical reactors and fuel injection in engines. These flows are characterized by a carrier phase bearing a dispersed phase in the form of particles, droplets or bubbles. The two distinct phases interact with each other, exchanging mass, momentum and energy, often occurring under turbulent conditions.

To investigate such a complex flow, fluid dynamicists have implemented a range of complementary computational approaches (Balachandar and Eaton, 2010; Brandt and Coletti, 2021). Briefly speaking, if the dimensional scale of the dispersed phase is significantly larger than the smallest scale of the carrier flow, a fully resolved method might be favourable to thoroughly address all scales of the carrier fluid and sub-particle scales necessary to capture the fluid/particle interface. The main restriction of a fully resolved resolution, from the perspective of computational cost, is the wide range of spatial–temporal scales and the limited amount of particles seeded into the carrier flow (Ardekani et al., 2016; Burton and Eaton, 2005). On the other hand, the Eulerian approach, treating the collection of droplets/particles as an interpenetrating continuum as the carrier one, relaxes the limitation of computational cost to some extent (Druzhinin and Elghobashi, 1998; Balachandar and Eaton, 2010). This approximation, however, might not provide accurate predictions, especially in the case that a particulate phase with an extensive variety of sizes is of interest (Fox et al., 2008).

When restricting the focus on particles/droplets smaller than the dissipative length scales, the most suitable numerical approach for addressing the problem relies on the Eulerian–Lagrangian framework. In the latter, individual particles/droplets are tracked with several degrees of freedom describing their properties like position, size and velocity under the *point-particle approximation* (Dukowicz, 1980; Squires and Eaton, 1990; Subramaniam, 2013). The attraction lies in the relaxed geometric coupling between the fluid and the suspended particles, which means that enforcement of the no-slip and no-penetration boundary conditions, at the interface between the particles and the fluid, is no longer necessary (Balachandar et al., 2019). Each particle/droplet is tracked independently along its trajectory whereas the sub-particle-scale interactions between the particles/droplets and the surrounding

* Corresponding author.
E-mail addresses: jietuo.wang@poliba.it (J. Wang), federico.dallabarba@unipd.it (F. Dalla Barba).

https://doi.org/10.1016/j.ijmultiphaseflow.2023.104609
Received 26 April 2023; Received in revised form 4 August 2023; Accepted 7 September 2023
Available online 11 September 2023

carrier are not resolved. That indicates the necessity of models to close the evolution equation of the dispersed phase (Maxey and Riley, 1983). This strategy has the advantage of explicitly accounting for the continuum dynamics of the carrier flow and simultaneously considering the non-continuum physics of the dispersed phase as well. It is especially favourable when the polydispersity of the dispersed phase introduces a wide range of time and length scales. Nevertheless, interesting challenges will appear in the Eulerian–Lagrangian approach concerning the inter-phase transfer terms that couple the Lagrangian particle representations to the Eulerian gas-phase equations (Balachandar, 2009; Balachandar et al., 2019; Gualtieri et al., 2015). In standard practice, the effects of the dispersed phase on the gaseous phase are typically accounted for through several sink/source coupling terms. An accurate calculation of these terms is crucial for the correct prediction of physical behaviours. However, a common procedure of estimating the coupling terms considers only Lagrangian particles in the domain location they occupy. In other words, the exertion of dispersed source terms on the Eulerian phase is localized within the grid cell enveloping the particle, which makes the approach not independent of grid-based particle number density. Especially considering that the spatial distribution of physical particles is highly nonuniform in many multiphase systems, a careful implementation of this numerical parameter could be a necessity to guarantee converged results. One simple method alleviating this issue may be increasing the number of particles/droplets (Garg et al., 2009; Balachandar, 2009) whereas the computational cost associated with the Eulerian–Lagrangian approach also grows linearly with the number of particles/droplets (Johnson, 2020).

Thanks to the modern advancement in computer technology, we can have access to detailed time- and space-resolved quantities in systems with thousands of millions of particles/droplets. However, in the case of billions or more particles, or computational resources being strictly capped, which is not uncommon, an Eulerian–Lagrangian approach could be prohibitively difficult for practical applications. A straightforward way of alleviating this issue could be achieved by simply representing a group of physical particles/droplets with the same properties as a single computational particle/droplet (Dukowicz, 1980; Mostafa and Mongia, 1987; Amsden et al., 1989; Elghobashi, 1994; Sankaran and Menon, 2002; Apte et al., 2003; Okong'o and Bellan, 2004; Salewski, 2006), referred to as *parcel*. This technique consists of lowering the degrees of freedom of the system and is analogous to the Eulerian coarse-graining (an increase of mesh size) moving from Direct Numerical Simulation (DNS) to Large-eddy Simulation (LES). Since the reduction of tracked particles/droplets inevitably leads to estimation errors (Subramaniam, 2013), implementing such a method always aims to reproduce the requested flow statistics accurately.

In the following a brief review of the evolution of the parcel concept is provided. Varying the number of computational particles (parcels), in reality, will result in a trade-off relationship between the statistical accuracy of the calculation and the computational time and storage. This has been reported, probably for the first time, by Dukowicz (1980) in studying the effect of particle number on the shape and penetration of sprays. Afterwards, aiming to evaluate both the Eulerian and Lagrangian approaches in modelling the turbulent evaporating sprays, Mostafa and Mongia (1987) analysed the sensitivity of the spray dynamics on the parcel concept by progressively increasing the total amount of computational droplets. This was done until only 3% difference has accrued when using the optimal number and the next higher one.

Amsden et al. (1989), in the KIVA-II code, associated the number of real particles/droplets to the parcel as a numerical weight in the context of droplet coalescence in sprays, which is still the basis of most engine spray CFD modelling package. Sankaran and Menon (2002) tracked 10^5 computational particles in performing LESs of spray combustion and justified this number as large enough to obtain accurate droplet statistics.

Focusing on simulating a temporal mixing layer laden with evaporating droplets under the Eulerian–Lagrangian framework, Okong'o and Bellan (2004) evaluated the capability of LES to replicate the detailed characteristics of a DNS. They considered seven parcel-ratio cases in which one computational particle represents 1, 2, 4, 8, 16, 32, 64 physical droplets, respectively. In addition, they considered two reduced flow field resolutions, i.e., a grid spacing four/eight times larger than that of the DNS. Moreover, different models for resolved source terms and unfiltered *sgs* fluxes were also taken into the assessment. They reported a complex dependence correlation between the filtering size and the number of computational droplets when comparing the relative error of modelling the unresolved flow field with that of the parcel concept. Interestingly, a progressive reduction of the computational droplets leads to a deterioration of the performance of LES models, and finally, the modelling error becomes independent of the filter width.

Salewski (2006) performed LESs of sprays issued into a cross-flow with 4500, 11000, 28000, and 54000 computational evaporating droplets. By examining quantities such as the liquid fractional volume and the drop size distribution, they concluded that no remarkable difference between solutions exists when the number of droplets is increased beyond 11000. Radhakrishnan and Bellan (2012) suspected that such a justification might not hold for higher-order statistics such as scalar fluxes.

To quantify the influence of the number of computational droplets and filtering width on accurately predicting flow statistics, as well as to identify the optimal number of computational drops that provide minimal errors in flow prediction, Radhakrishnan and Bellan (2012) performed LESs of a mixing layer with evaporating droplets. They increased the number of computational droplets with a parcel ratio varying from 8 to 128 of physical particles in conjunction with two different filter width, i.e. a fine and a coarse mesh grid. They reported the second-order flow statistics' dependency on both the computational droplet number and the filter size. In particular, they showed that the number of computational droplets tracked in the fine-mesh LES simulations could be reduced by a factor of no more than *32* as compared to the correspondent DNS without reducing the accuracy of scalar variance and turbulent vapour flux. When a significant representation factor of computational droplets was used, the coarse-mesh LESs provided reasonably accurate predictions, whereas the fine-mesh ones were not as accurate as their counterpart.

Besides, the parcel concept has been also widely adopted in research focusing on the breakup or collision of droplet/particles (Patankar and Joseph, 2001; Apte et al., 2003, 2009; Alobaid, 2015; Johnson, 2020).

Even if investigations employing the parcel concept have been carried out widely, a well-established criterion for choosing the representation factor of parcel/computational droplet in relation to the mesh spacing is still waiting to be determined. Also, the database of implementing the parcel concept with respect to evaporating droplets in high-Re turbulent sprays needs to be included. To cover these scientific gaps, we address a series of well-resolved Large-eddy Simulations of a turbulent diluted acetone jet-spray considering different ratios of computation droplets to physical droplets, i.e., parcel ratio, in conjunction with two different grid spacings. The numerical tool is a validated MPI parallel code which solves the low-Mach number formulation of Navier–Stokes equations on a cylindrical domain coupled with a Lagrangian solver to deal with the position, velocity, radius and temperature of point-droplets. By benchmarking against LESs using only physical droplets and a corresponding fully resolved DNS, we quantify the influence of the parcel ratio and grid spacing on accurately and efficaciously reproducing the statistics of both carrier and dispersed phases and identify the threshold that provides minimal errors.

More specifically, the principal aim of the present paper is to assess a precise criterion to choose the parcel ratio in an LES of a turbulent, evaporating spray involving a parcel model. This is done by assessing the quality of different statistics and observables reproduced in LESs with different parcel ratios and resolutions. The authors believe that the

outcome of the present work could be twofold: a criterion for choosing the parcel ratio without affecting the statistics of the flow could give rise to the possibility of affording the simulations of flows of practical interest involving billions of evaporating droplets; the dataset presented in the present paper could be useful to evaluate to which extent the usage of a parcel model affects the statistics of a turbulent evaporating spray.

2. Numerical methodology

2.1. Formulation

The present work uses a hybrid Eulerian–Lagrangian technique with the two-way coupling method to simulate dilute turbulent sprays within the large eddy simulation framework. The velocity, vapour mass fraction, temperature and density fields of the carrier phase are described with an Eulerian approach, whereas the droplets are treated in a Lagrangian manner by employing the well-established point-wise approximation. The governing equations are solved in cylindrical coordinates in an open environment at constant pressure, p_0. Given these hypotheses, the governing equations, after, applying the Favre-weighted filtering (Favre, 1983) to the asymptotic low-Mach expansion of the Navier–Stokes and energy formulas, can be written as in the following:

$$\frac{\partial \overline{\rho}}{\partial t} + \frac{\partial \overline{\rho}\tilde{u}_i}{\partial x_i} = \overline{S}_m\,, \tag{1}$$

$$\frac{\partial \overline{\rho}\tilde{u}_i}{\partial t} + \frac{\partial \overline{\rho}\tilde{u}_i\tilde{u}_j}{\partial x_j} = -\frac{\partial \overline{p}}{\partial x_i} + \frac{\partial}{\partial x_j}\left[(\mu_g + \mu_{sgs})\left(\frac{\partial \tilde{u}_i}{\partial x_j} + \frac{\partial \tilde{u}_j}{\partial x_i} - \frac{2}{3}\frac{\partial \tilde{u}_i}{\partial x_i}\delta_{ij}\right)\right] + \overline{S}_{p,i}\,, \tag{2}$$

$$\frac{\partial \overline{\rho}\tilde{Y}_v}{\partial t} + \frac{\partial \overline{\rho}\tilde{Y}_v\tilde{u}_i}{\partial x_i} = \frac{\partial}{\partial x_i}\left(\overline{\rho}(D + D_{sgs})\frac{\partial \tilde{Y}_v}{\partial x_i}\right) + \overline{S}_m\,, \tag{3}$$

$$\frac{\partial \tilde{u}_i}{\partial x_i} = \frac{\gamma - 1}{\gamma}\frac{1}{p_0}\left[\frac{\partial}{\partial x_i}\left((\kappa_g + \kappa_{sgs})\frac{\partial \tilde{T}}{\partial x_i}\right) + \overline{S}_e - L_v\overline{S}_m\right]\,, \tag{4}$$

$$p_0 = \tilde{T}\overline{\rho}R_g\,, \tag{5}$$

where $\overline{\rho}$, $\tilde{u}_i$, $\tilde{Y}_v$, $\tilde{T}$ and $\overline{p}$ are the density, *i-th* velocity, vapour mass fraction, temperature and hydrodynamic pressure of the flow field, respectively. The parameter μ_g refers to the dynamic viscosity of the gaseous phase, and D is the binary mass diffusion coefficient. κ_g is the thermal conductivity of the vapour-air mixture while L_v indicates the latent heat of vaporization of the liquid phase. The carrier phase is assumingly governed by the equation of state for ideal gases where $R_g = R/W_g$ is the gas constant of the mixture, with W_g being its molar mass and R the universal gas constant. The parameter $\gamma = c_{p,g}/c_{v,g}$ indicates the specific heat ratio of the carrier mixture where $c_{p,g}$ and $c_{v,g}$ are the gaseous phase specific heat capacity at constant pressure and volume, respectively. The subgrid-scale terms of the Navier–Stokes equation are described using the classical Smagorinsky model (Smagorinsky, 1963):

$$\mu_{sgs} = \overline{\rho}(C_s\Delta)^2\left\|\frac{1}{2}\left(\frac{\partial \tilde{u}_i}{\partial x_j} + \frac{\partial \tilde{u}_j}{\partial x_i}\right)\right\|\,, \tag{6}$$

where C_s is a model constant (0.12 in our setup) and $\Delta = [(r\Delta_\theta)\Delta_r\Delta_z]^{1/3}$ is the equivalent cell size. For subgrid-scale fluxes, D_{sgs} and κ_{sgs}, we adopt the gradient model proposed in Schmidt and Schumann (1989). Within this approach those two variables are evaluated by multiplying the Smagorinsky eddy-viscosity with constant turbulent Schmidt and Prandtl numbers, $Sc_t = 0.7$ and $Pr_t = 0.7$, respectively.

The effects of the dispersed phase on the gaseous phase are accounted for through three sink-source coupling terms (i.e. $\overline{S}_m$ for mass, $\overline{S}_{p,i}$ for momentum and $\overline{S}_e$ for energy):

$$\overline{S}_m = \frac{PR}{\Delta^3}\sum_{k=1}^{n_d} -\frac{dm_k}{dt}\delta(x_i - x_{k,i})\,, \tag{7}$$

$$\overline{S}_{p,i} = \frac{PR}{\Delta^3}\sum_{k=1}^{n_d} -\frac{d}{dt}(m_k u_{k,i})\delta(x_i - x_{k,i})\,, \tag{8}$$

$$\overline{S}_e = \frac{PR}{\Delta^3}\sum_{k=1}^{n_d} -\frac{d}{dt}(m_k c_l T_k)\delta(x_i - x_{k,i})\,, \tag{9}$$

where $x_{k,i}$, m_k, $u_{k,i}$ and T_k are the *i-th* position component, mass, *i-th* velocity component and temperature of the *k-th* computational parcel. c_l is the liquid specific heat.

It is noteworthy that, in the present work, a distinction exists between physical droplets and parcels, though both are described with the point-particle approximation. A parcel is defined as a computational particle representing the dynamics of a given number of physical droplets. In this context, the parameter *PR* (parcel-ratio) used in this study indicates the number of physical droplets represented by a parcel. The summations in Eqs. (7)–(9) are taken over the entire domain populating parcels (being n_d the total number). The delta function expresses the fact that the sink-source terms act only at the domain location occupied by the parcels. These terms are calculated in correspondence with each grid node by volume-averaging the mass, momentum, and energy sources from all parcels located within the cell volume centred around the considered grid point. Noteworthy is that, such a standard practice of accounting the inter-phase transfer terms within the Eulerian–Lagrangian framework principally has two drawbacks: one relies on the accumulation of the spread quantities, such as the vapour concentration, within a single computational cell and the other relies on the self-sampling of the spread quantities by each droplet/parcel (Gualtieri et al., 2015; Horwitz and Mani, 2018; Balachandar et al., 2019). That may exert an influence on the parcel ratio threshold to be investigated. Even if different approaches exist to treat these drawbacks for single droplet, the issue becomes more complicated in the case of parcels. On the other hand, this approach, a step-back from the progressively increasing complexity of modelling multiphase flows, has been demonstrated to provide good results in all our previous works (Picano et al., 2010; Rocco et al., 2015; Dalla Barba and Picano, 2018; Ciottoli et al., 2021; Wang et al., 2021b,a).

The evolution of the dispersed phase is described in the Lagrangian frame. In particular, the size of the evaporating droplets considered in the present work is assumed to be small enough (below the dissipative length scale) to be treated as rigid evaporating spheres and approximated as point-wise droplets. In addition, the temperature of the liquid phase is assumed to be uniform inside each droplet. As the volume (and mass) fraction of the liquid phase considered in the present study is relatively small, the mutual interactions among droplets (i.e. collisions and coalescence) can be neglected. Besides, the effect of the subgrid-scale terms is not taken into consideration. Hence, only the resolved part of the Eulerian fields is used in the equations of the dispersed phase. Within these assumptions, the position, velocity, mass and temperature of the droplets are described by the following equations:

$$\frac{dx_{k,i}}{dt} = u_{k,i}\,, \tag{10}$$

$$\frac{du_{k,i}}{dt} = \frac{(\tilde{u}_i - u_{k,i})}{\tau_k}(1 + 0.15Re_k^{0.687}), \tag{11}$$

$$\frac{dr_k^2}{dt} = -\frac{\mu_g}{\rho_l}\frac{Sh}{Sc}\ln(1 + B_m)\,, \tag{12}$$

$$\frac{dT_k}{dt} = \frac{1}{3\tau_k}\left[\frac{Nu}{Pr}\frac{c_{p,g}}{c_l}(\tilde{T} - T_k) - \frac{Sh}{Sc}\frac{L_v}{c_l}\ln(1 + B_m)\right]\,, \tag{13}$$

where $x_{k,i}$, $u_{k,i}$, r_k and T_k are the position, velocity, radius and temperature of the *k-th* droplet while ρ_l is the liquid density. The droplet relaxation time, τ_k, and the droplet Reynolds number, Re_k, are defined as:

$$\tau_k = \frac{2\rho_l r_k^2}{9\mu_g}\,, \qquad Re_k = \frac{2\rho_l\|\tilde{u}_i - u_{k,i}\|r_k}{\mu_g}\,, \tag{14}$$

while the Schmidt number, Sc, and Prandtl number, Pr, are computed as:

$$Sc = \frac{\mu_g}{\rho_g D}, \qquad Pr = \frac{\mu_g c_{p,g}}{k_g}, \tag{15}$$

where μ_g and ρ_g indicate the dynamic viscosity and density of the gaseous phase, respectively. D is the binary mass diffusion coefficient and κ_g is the thermal conductivity. The Sherwood number, Sh, and Nusselt number, Nu, are estimated as a function of the droplet Reynolds number using the Frössling correlations (Froessling, 1968):

$$Sh_0 = 2 + 0.552 Re_k^{1/2} Sc^{1/3}, \qquad Nu_0 = 2 + 0.552 Re_k^{1/2} Pr^{1/3}. \tag{16}$$

The resulting Sherwood and Nusselt numbers are corrected to account for the Stefan flow (Abramzon and Sirignano, 1989; Dalla Barba and Picano, 2018):

$$Sh = 2 + \frac{Sh_0 - 2}{F_m}, \qquad Nu = 2 + \frac{Nu_0 - 2}{F_t}. \tag{17}$$

The coefficients F_m and F_t are computed as follows:

$$F_m = \frac{(1 + B_m)^{0.7}}{B_m} H_m, \qquad F_t = \frac{(1 + B_t)^{0.7}}{B_t} H_t, \tag{18}$$

where H_m and H_t are defined as:

$$H_m = \ln(1 + B_m), \qquad H_t = \ln(1 + B_t), \tag{19}$$

being B_m and B_t the Spalding mass and heat transfer numbers (Spalding, 1950):

$$B_m = \frac{Y_{v,s} - \tilde{Y}_v}{1 - Y_{v,s}}, \qquad B_t = \frac{c_{p,v}}{L_v}(\tilde{T} - T_k), \tag{20}$$

where $\tilde{Y}_v$ and $\tilde{T}$ are the vapour mass fraction and temperature fields evaluated at the droplet position, $Y_{v,s}$ is the vapour mass fraction evaluated at the droplet surface and $c_{p,v}$ is the vapour specific heat at constant pressure. The vapour mass fraction at the droplet surface corresponds to the mass fraction of the vapour in a saturated vapour–gas mixture at the droplet temperature. To estimate $Y_{v,s}$, we use the Clausius–Clapeyron relation to compute the vapour molar fraction, $\mathcal{X}_{v,s}$:

$$\mathcal{X}_{v,s} = \frac{p_{ref}}{p_0} \exp\left[\frac{L_v}{R_v}\left(\frac{1}{T_{ref}} - \frac{1}{T_k}\right)\right], \tag{21}$$

where p_{ref} and T_{ref} are arbitrary reference pressure and temperature and $R_v = R/W_l$ is the vapour–gas constant. The saturated vapour mass fraction is then computed using the following relation:

$$Y_{v,s} = \frac{\mathcal{X}_{v,s}}{\mathcal{X}_{v,s} + (1 - \mathcal{X}_{v,s})\dfrac{W_g}{W_l}}, \tag{22}$$

where W_g and W_l are the molar mass of the gaseous and liquid phases, respectively. The procedure for non-dimensionalization and low-Mach number approximation is skipped in this paper. For those interested, please check (Dalla Barba, 2016; Wang, 2022).

2.2. Tools and simulation setup

The numerical experiments were performed by employing an in-house MPI-parallel code, *CYCLON*, which has undergone extensive validations and test campaigns (Picano et al., 2010; Rocco et al., 2015; Dalla Barba and Picano, 2018; Ciottoli et al., 2021; Wang et al., 2021b,a). This numerical algorithm consists of two main parts. An Eulerian algorithm is dedicated to advance in time the flow fields by solving the Low-Mach number formulations of the Navier–Stokes equations. A Lagrangian solver is designed to synchronously evolve the mass, momentum, and temperature equations of dispersed droplets under point-particle approximation. The Lagrangian solver also estimates the coupling terms arising in the spray equations, granting a full coupling between the carrier flows and the liquid phase.

Table 1
Thermodynamic and physical properties of acetone and dry air, reference length scale time scale and velocity scale.

R	0.0049 [m]	W_g	0.029 [kg/mol]
p_0	101 300 [Pa]	W_l	0.0581 [kg/mol]
T_0	275.15 [K]	k_g	0.0243 [W/(m K)]
μ	1.75 E−5 [kg/(m s]	k_l	0.183 [W/(m K)]
$c_{p,g}$	1038 [J/(kg K)]	D	1.1E−5 [m^2/s]
$c_{p,v}$	1300 [J/(kg K)]	ρ_l	800 [kg/m^3]
c_l	2150 [J/(kg K)]	L_v	530 000 [J/kg]
U_0	13.9 [m/s]	r_d	6E−6 [m]
t_0	3.5E−4 [s]		

For the Eulerian algorithm, a second-order, central finite difference scheme on a staggered cylindrical mesh is employed for the spatial discretization, whereas a low-storage, third-order Runge–Kutta algorithm performs the temporal evolution. The same Runge–Kutta scheme is adopted to advance the Lagrangian phase in time. A second-order accurate polynomial interpolation is used to evaluate the Eulerian quantities at the droplet position. Besides, the numerical tool engages MPI directives in order to maximize computational performance. More details, benchmarks and tests can be found in Dalla Barba and Picano (2018), Ciottoli et al. (2021) and Wang et al. (2021b).

The computational domain is a cylinder (see Fig. 1). The droplet-laden jet-spray is issued through a circular orifice of radius R located at the centre of the lower base of the domain and streams out towards the opposite direction. The cylinder dimension extends in the azimuthal (θ), radial (r) and axial (z) directions, respectively, with $L_\theta \times L_r \times L_z = 2\pi \times 20R \times 70R$. The domain is discretized in a staggered way such that the computational grid is uniform along the azimuthal direction and stretched along the other two directions.

Two mesh configurations are generated by reducing by a factor 4/8 in each direction the grid points of a reference Direct Numerical Simulation (DNS) mesh (see Wang et al. (2021b)), i.e. a fine mesh with $N_\theta \times N_r \times N_z = 48 \times 54 \times 288$ grid points and a coarse mesh with $N_\theta \times N_r \times N_z = 24 \times 26 \times 144$ grid points. Regarding the inflow section, we prescribe time-dependent and fully turbulent boundary conditions by employing a companion DNS reproducing a fully-developed, periodic pipe flow (Fig. 1.c). The pipe domain, which extends for $2\pi \times 1R \times 6R$ in the azimuthal, θ, radial, r and axial, z, directions, is discretized in such a way that the equispaced, staggered mesh matches the corresponding jet computational grid at the pipe discharge. A convective boundary condition is adopted on the outlet section located on the upper face of the cylindrical domain, and an adiabatic, traction-free boundary condition is prescribed at the domain's side boundary, making possible the entrainment of external fluids which consists of dry air in the present study. Besides, a fully turbulent velocity field is assigned to the jet inflow by a Dirichlet condition. That means this two-dimensional field is computed on a cross-sectional slice of the turbulent pipe. Excluding the circular inflow, the remaining part of the domain base is impermeable and adiabatic. It is noteworthy that the use of a companion pipe simulation makes it possible to prescribe fully turbulent inflow conditions, including physically meaningful turbulent fluctuations.

The present work simulates the dynamics of liquid acetone droplets dispersed within a turbulent air-acetone vapour jet within a Large Eddy Simulation (LES) framework. The gas–vapour mixture is injected into an open environment through an orifice of radius $R = 4.9 \times 10^{-3}$ m at a bulk velocity $U_0 = 13.9$ m/s. Mono-dispersed acetone parcels/droplets with an initial radius $r_{d,0} = 6$ μm are randomly released over the inflow section. The injection velocity of each parcel/droplet is prescribed as the same value as the local velocity of the turbulent carrier phase. The ambient pressure is set to $p_0 = 101\,300$ Pa while the injection temperature is fixed to $T_0 = 275.15$ K for both the droplets and carrier mixture. The injection flow rate of the gaseous phase is kept constant, fixing a bulk Reynolds number $Re = 2U_0R/\nu = 10\,000$, with $\nu = 1.35 \times 10^{-5}$ m^2/s the kinematic viscosity. At the inflow section,

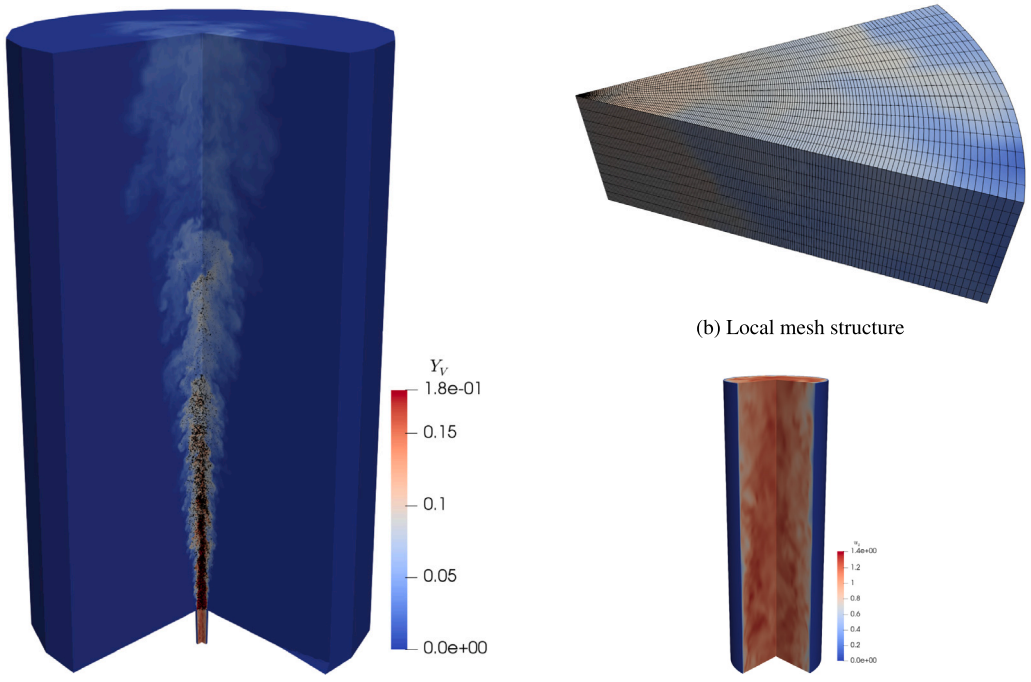

(a) 3D cylindrical domain (b) Local mesh structure (c) 3D pipe flow

Fig. 1. (a) A sketch of the 3D cylindrical domain where a representative ensemble of the whole droplet population is plotted with black points. (b) A local sector of the mesh structure centred at $z/R = 20$. (c) The turbulent periodic pipe. The colours contour the vapour mass fraction field, Y_v, within the jet and the axial instantaneous velocity, U_z, of the turbulent pipe, respectively. (For interpretation of the references to color in this figure legend, the reader is referred to the web version of this article.)

a nearly saturated condition is prescribed for the air-acetone vapour mixture, $S = Y_v/Y_{v,s} = 0.99$. In the latter, Y_v is the actual vapour mass fraction whereas $Y_{v,s}(p_0, T_0)$ is the vapour mass fraction saturation level evaluated at the actual inflow temperature and thermodynamic pressure. The acetone mass flow rate is set by the mass flow rate ratio $\Phi = \dot{m}_{act}/\dot{m}_{air} = 0.28$, with $\dot{m}_{act} = \dot{m}_{act,l} + \dot{m}_{act,v}$ the sum of liquid and vapour acetone mass flow rates and $\dot{m}_{air}$ the gaseous one. The correspondent bulk volume fraction of the liquid phase is set to $\Psi = 8 \times 10^{-5}$. All the thermodynamic and physical properties of the vapour, gas, and liquid phases are reported in Table 1.

The thermodynamic conditions at the inlet are comparable to that adopted in the well-controlled experiments on dilute coaxial sprays published by the group of Chen et al. (2006). Concerning the reliability of the simulations, some validation benchmarks considering the statistics of the turbulent periodic pipe and the corresponding single-phase jet DNS, as well as the evaporation model testing, can be found in Dalla Barba and Picano (2018).

3. Results and discussion

In this section we provide the data analysis of numerical simulations reproducing a turbulent jet-spray in the same physical conditions, but with different numerical arrangements. The essential differences between the reported simulations rely on the number of Eulerian grid nodes and Lagrangian parcels. In detail, we performed a total of six LESs with a *fine mesh*, (*e.g., LES4*, where the number denotes a reduction factor of 4 with respect to the reference DNS mesh), adopting a constant parcel ratio, PR, ranging within $[1, 4, 16, 64, 256, 1024]$. Additionally, five more LESs using a *coarse mesh*, *e.g. LES8*, were carried out by considering a constant but more aggressive PR spanning in the range $[1, 8, 64, 512, 4096]$. The DNS results from our previous work, Ref. Wang et al. (2021b), are employed as reference data. It is worth noting that, for both LES meshes, the PR values considered here have been selected attentively with the aim of clearly revealing their correlation with the reduction of the degree of freedom from the DNS to the LES meshes. To assess the effectiveness of parcel model implementation

Table 2
Core hours, t_{cpu}, memory/storage consumption, Mc, and parcels/droplets number per cell, N_{pc}, of $LES4$ and $LES8$ with different PR values.

LES4	PR	1	4	16	64	256	1024
	t_{cpu}	14.14	5.03	2.54	1.93	1.77	1.70
	Mc	311.5	100.3	48.8	35.7	32.6	31.8
	$\langle N_{pc} \rangle$	3.50	0.873	0.219	0.0545	0.0137	3.41×10^{-3}
LES8	PR	1	8	64	512	4096	
	t_{cpu}	11.54	1.46	0.24	0.15	0.14	
	Mc	255.4	35.8	8.4	4.9	4.5	
	$\langle N_{pc} \rangle$	27.7	3.45	0.432	0.0543	6.60×10^{-3}	

and computational resources, Table 2 provides a summary of three simulation statistics for each *LES* case. These statistics include core hours, t_{cpu}, memory storage consumption in Megabyte, Mc, and mean parcel/droplets density, $\langle N_{pc} \rangle$. The particles considered for this density calculation are those present close the inlet, specifically where $r/R < 1.0$ and $z/R < 1.0$, and they are collected for each time-instant. As a comparison, the corresponding statistics for the bechmarking DNS are 5038 (t_{cpu}), 2102.1 Mc and 0.0569 $\langle N_{pc} \rangle$, respectively. All the statistics, both in the table and the following sections, are computed considering around 100 samples separated in time by a time $R/U_0 = 1$ after reaching a statistically steady condition for the two-phase evaporating flows.

The spatial filtering concept in an LES approach inevitably leads to the loss of the small-scale details of the carrier flow, which will not be *felt* by the evaporating droplets/parcels as they evolve within the fluid domain (Marchioli, 2017). To this end, in Fig. 2, we provide the instantaneous flow field of the vapour mass fraction and the spatial distribution of the evaporating acetone droplets in the benchmarking DNS, *LES4* and *LES8* with $PR \in [1, 64]$, respectively. The panels qualitatively show the effect of the spatial filtering and PR. It is clear, at first glance, how increasing the filtering width progressively removes vortical information from the flow fields in the LESs. The general appearance of the contour levels and structures in $LES4_{PR001}$ fairly

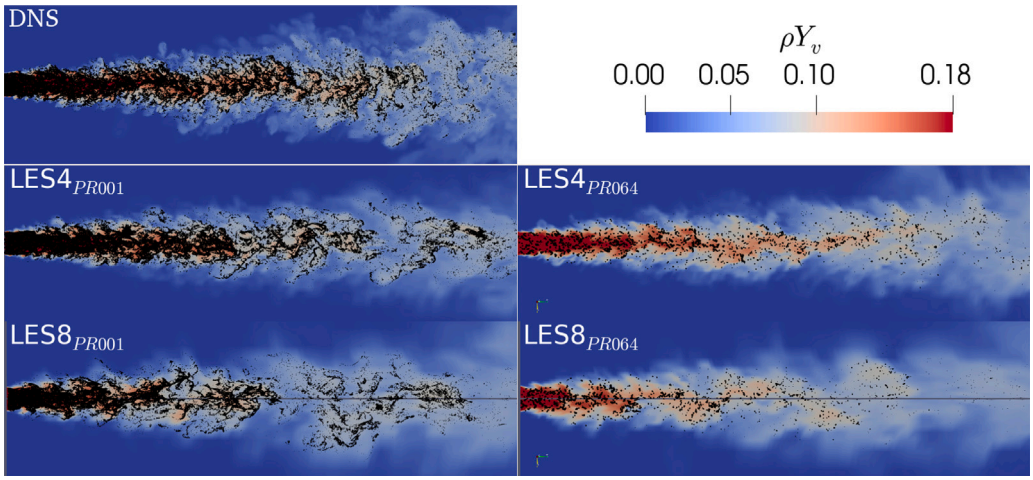

Fig. 2. Radial-axial slices of the turbulent sprays for the DNS and the LESs with a visualization scope along the axial direction of $0 < z/R < 45$. The black points represent a subset of the whole droplet population constituted by the droplets located within a distance $h/R = 0.1$ from the slice plane. The point size in the left panels is scaled by the corresponding droplet radius with a fixed scale factor of *50*. An appropriate enlargement is applied for the size of the points in the right panels for improved visualization. The carrier phase is contoured according to the instantaneous vapour mass fraction field, Y_v, which is bounded between 0 and 0.18, the former corresponding to the dry air condition and the latter to the 99% saturation level prescribed at the inlet. For perspicuity reasons, results of LESs with *PR = 1, 64* are shown here only.

approximate to the benchmarking DNS, whereas a shorter, wider and detail-blurry jet appears after filtering with the coarser LES mesh, i.e., red regions in $LES8_{PR001}$. The approximated flow fields resulting from the LES filtering scheme, together with the inaccuracies caused by the interpolation on coarse-grained domains, affect the estimation of the variables delivered to the Lagrangian equations of droplet movement and evaporation. This effect may accumulate in time and space, which means that the flow fields *felt* by droplets become less and less correlated, and the forces acting on particles are evaluated at increasingly different locations, resulting in an increasingly different trajectory and lifetime of droplets (Marchioli, 2017).

The apparent small-scale clusters of evaporating droplets displayed in the DNS panel, which strongly correlates with regions with high vapour concentration (Dalla Barba and Picano, 2018; Wang et al., 2021b), are to some extent successfully reproduced by the $LES4_{PR001}$, despite at larger spatial scales. In contrast, the replication of these small-scale clusters is hardly observed in the $LES8_{PR001}$ since the velocity fields and localized vapour concentration *felt* by the droplets become more and more divergent from the reference DNS. On the other hand, the implementation of computational parcels, instead of physical droplets, does not exert a noticeable influence on the carrier flow in this dilute regime, as shown in the right panels of Fig. 2, but loses the highly spatial non-uniformity of dispersed droplets, potentially leading to numerical errors as suggested in Subramaniam (2013).

Besides the instantaneous distribution of single realizations of LESs, additional insights about the robustness of the parcel model can be gained from the statistical moments, e.g., averages and Joint Probability Distribution Functions (JPDFs). In Fig. 3(a), we compare the average distribution of the liquid mass fraction normalized by the initial value, $\langle \Phi/\Phi_0 \rangle$, between the LESs with physical droplets and with parcel concept at different *PR* values. The mass fraction is determined by $\Phi = m_l/m_g$, where m_l and m_g are the mass of liquid acetone and of the gaseous phase evaluated inside each mesh cell. It is essential to note that the maximum mass (and volume) fractions of the liquid phase for each case are consistent, with a value of 0.052 ($8 \times 10^{-}5$), which is prescribed as the inflow condition, i.e. Φ_0 (Ψ_0). When the parcel model is used, fewer individual particles are visualizable; however, the inflow mass(volume) fraction remains the same since a parcel represents a group of physical particles. To quantitatively assess the evaporation completeness, we define the spray vaporization length as the axial distance from the inlet section to the position where the mean liquid mass fraction decreases to 1% with respect to the prescribed value at the inlet region. In other words, the droplets/parcels lose 99% of their initial mass, on average. According to this definition, in Fig. 3(a), we show that the vaporization process completes at about $z/R \sim 52$, $z/R \sim 51$, $z/R \sim 52$, $z/R \sim 50$, $z/R \sim 53$, and $z/R \sim 60$ for *LES4* with increasing *PR* value from *1* to *1024*, and $z/R \sim 42$, $z/R \sim 42$, $z/R \sim 43$, $z/R \sim 43$, and $z/R \sim 52$ for *LES8* with enlarging *PR* value from *1* to *4096*. At first glance, the overall distribution of $\langle \Phi/\Phi_0 \rangle$ is not eminently affected by setting small values to PR, but it is progressively elongated after PR reaches a certain threshold. Another interesting point is that the LES performed with a coarser mesh, *LES8*, seems less sensitive to the parcel model with respect to the *LES4* case. For the former, a higher limit of the *PR* value is observable before the evaporation length strongly deviates from the reference. In this sense, the LES approach with a coarse filtering grid presents an improved compatibility in the coupling with the parcel model.

In Figs. 3(b) and 3(c) we show additional comparisons of the spatial distribution of $\langle \Phi/\Phi_0 \rangle$ along the centre-line of the jet-spray, i.e., $r/R < 0.2$. The statistics are provided at three different z/R positions, i.e., $z/R = 5, 25, 45$, for both *LES4* and *LES8* with different *PR* values, accompanied by the correspondent DNS data as a benchmark. It is evident that, for all cases displayed, the overall trend is the same. For instance, in the centre-line plot, the liquid mass fraction increases along the jet-axis from the inflow section up to a peak at $z/R \simeq 11$ for *LES4* and $z/R \simeq 6$ for *LES8*. This behaviour is consistent with the observations by Picano et al. (2010) and Lau and Nathan (2014, 2016) in which the centreline concentration of inertial particles is found to increase above the injection value. This phenomenon is explainable by considering the interplay of the droplet/parcel inertia and the decay of the mean fluid velocity. The inertia induces a delay of the droplet velocity to adapt to the slower (decayed) flow velocity. This creates a local concentration peak, which becomes weaker in the presence of a coarse filtering grid due to the faster evaporation shown in Fig. 5. Further downstream, $\langle \Phi/\Phi_0 \rangle$ reduces along the jet-axis until droplets/parcels completely evaporate.

The *LES4* results with parcel ratios up to $PR = 64$ replicate well the vaporization length and radial distributions of $\langle \Phi/\Phi_0 \rangle$ with respect to the benchmarking DNS result. On the other hand, a significant deviation starts to appear in the intermediate- and far-fields of both the outer and inner regions when the parcel ratio increases, i.e., *PR = 256* or *PR = 1024*. The vaporization length of the LES4 with the highest parcel ratio is about 20% longer than that of the benchmarking DNS. This fact can be explained by considering that, as the parcel ratio increases, fewer parcels are available in each cell to form the mesh-based average statistics. Hence, the statistical errors, which are inversely

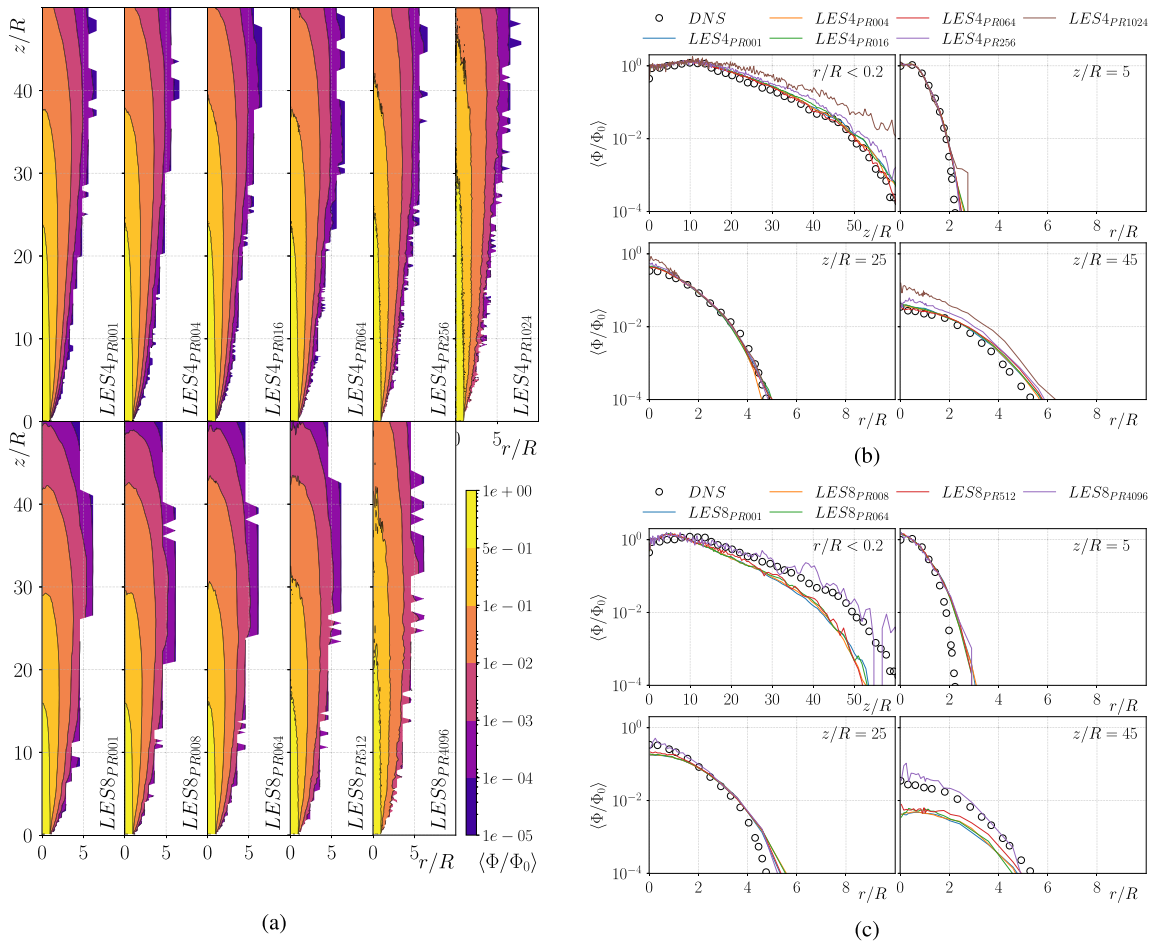

Fig. 3. (a) Mean liquid mass fraction, $\langle \Phi \rangle = m_l/m_g$, normalized by the initial value Φ_0, where m_l and m_g are the mean mass of liquid acetone and air inside each mesh cell, respectively. LESs with two mesh configurations and different *PR* values are shown. (b) and (c) show the $\langle \Phi/\Phi_0 \rangle$ distribution along the centre axis, $r/R < 0.2$, and three different z/R positions, *e.g.* z/R = 5, 25, 45, for all LESs which are accompanied by DNS data as a benchmark.

proportional to the square root of the parcel number per cell, would progressively increase (Subramaniam, 2013). This potentially leads to an underestimation of the evaporation rate of the droplets/parcels. In fact, in the LES4 cases with the higher *PR*, the parcel in a computational cell may impose on the carrier flows an excessive source of mass, momentum and energy, leading to localized regions with high vapour concentrations which eventually slows down the evaporation process of the droplets/parcels. Moving downstream from the origin, the error induced by the parcel representation of the droplets tends to accumulate, leading to less accurate statistics. Interestingly, with a higher parcel ratio in a lower accurate LES, e.g., $LES8_{PR4096}$ (purple curve in 3(c)), the mean distribution of Φ/Φ_0 is more proximate to that of the reference DNS compared to other *PR* values with the same filtering space. In particular, $LES8$ simulations with parcel ratio up to 512 present a vaporization length close to that of the case considering only physical droplets, $PR = 1$, which is 16% shorter than that of the reference DNS. It is natural to speculate that the errors caused by the larger filter could be offset by those introduced by the aggressive parcel model, leading to improved statistics concerning the spatial distribution of the liquid mass fraction.

In Fig. 4(a), the spatial distribution of the average saturation level, S_v, is provided and compared among *LESs*. For both *LES4* and *LES8* simulations, the flow is almost saturated close to the inlet region due to the prescribed inflow conditions. Towards the downstream direction, the saturation level steadily diminishes, presenting a sharper gradient along the radial direction. The main difference between *LES4* and *LES8* relies on the truncated saturation field with the coarse mesh, i.e., *LES8*. We suppose this is caused by the nonphysically increased entrainment of dry air from the ambient induced by the larger filter width in *LES8*. Varying the parcel ratio, the spatial distribution of the average saturation level shows a limited response. This is reasonable by considering that the filter width is determinant regarding the accuracy of the numerical reproduction of the flow field, whereas droplet/parcel evaporation in dilute regimes plays a minor role in regulating the average saturation level with respect to its Eulerian counterpart, i.e., entrainment. Though the saturation level shows insignificant dependence on the *PR* model, the spatial distribution of the droplet/parcel size is indeed conditioned by the *PR* value. As shown in Fig. 4(b), the mean radius field of droplets/parcels extends longer along the axial direction, with respect to the reference case, after the *PR* reaches a specific threshold which is $PR = 64$ for the fine mesh and $PR = 512$ for the coarse mesh.

In such an initially saturated turbulent spray, the distinguished distribution of liquid mass fraction and droplets/parcel size could be traced back to the evaporation process. To this end, in Fig. 5(a), we provide a global comparison of the average distribution of the droplet/parcel evaporation rate normalized by the reference scale, $\dot{m}_{d,0} = m_{d,0}/t_0$. The quantity $m_{d,0}$ is the initial droplet mass whereas $t_0 = R/U_0$ is the reference time scale. The figure includes the statistics for both the LESs with the two mesh configurations and the different *PR* values. Near the inflow section, the evaporation rate of the droplets/parcels peaks in correspondence with the mixing layer that separates the jet core, with a higher saturation level, and the outer jet regions surrounded by the droplet-free ambient. The entrained dry

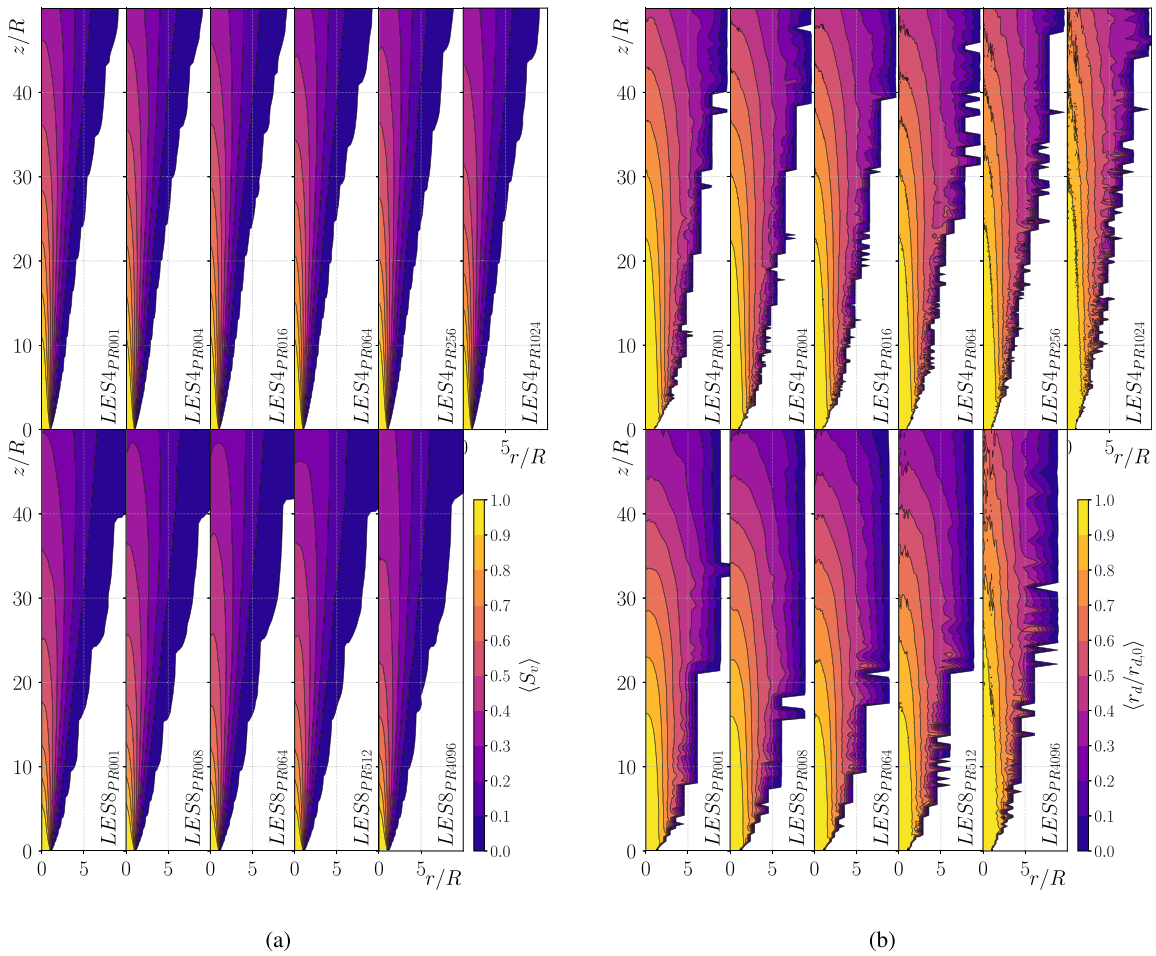

Fig. 4. (a) Average saturation field, $\langle S_v \rangle = \langle Y_v / Y_{v,s} \rangle$, where Y_v is the actual vapour mass fraction, and $Y_{v,s}$ is the value of the vapour mass fraction corresponding to the local saturation condition. (b) Mean droplet radius, $\langle r_d \rangle$, rescaled by the droplet initial radius $r_{d,0} = 6$ μm. The results of LESs with two mesh configurations and different *PR* values are present here.

air is not capable of reaching the fully saturated inner core in the proximity of the jet inlet region, leading to a lower intensity of the evaporation rate in the nearly-saturated core. This effect is to some extent impaired, as shown for the *LES8* cases, due to the numerical error originating from the larger filter. Hence, for *LES8*, we observe a broader mixing layer surrounding a shorter inner core with respect to *LES4*. As explained in Dalla Barba and Picano (2018) and Wang et al. (2021b), the irrotational ambient dry air, which is continuously entrained into the jet, dilutes the vapour concentration and facilitates the overall vaporization process to proceed during the spreading and decaying evolution of the turbulent jet. Moving downstream from the jet inflow, the region characterized by the higher level of the evaporation rate shifts to the core zone that transports the remaining larger droplets/parcels. By increasing the *PR*, the inner core region with highly saturated mixtures extends slightly longer along the stream-wise direction and is neighboured by a shrunk region where the evaporation rate peaks (the yellow contour area). This may be attributed to the fact that each parcel imposes the localized cell mass and moment source terms equivalent to that of the physical droplets represented by it.

In Figs. 5(b) and 5(c), we show the local distribution of the evaporation rate of the droplets/parcels along the centre line, $r/R < 0.2$, and at three different z/R positions indicating near-, intermediate- and far-fields, respectively, for all LESs. DNS data from our previous work (Wang et al., 2021b) are also shown as a benchmark. It is clear that, with the fine mesh, the evaporation rate of the droplets/parcels is almost identical or fairly approximate to the benchmarking DNS until $PR = 64$. Beyond this threshold, significant deviations along the whole spray are observable, revealing an attenuated evaporation process, especially along the centreline and at the near field. In contrast, in *LES8*, droplets/parcels start to evaporate faster at an axial distance from the jet inflow section which is shorter than that of the benchmarking DNS. In the authors' opinion, this may be induced by the nonphysically increased entrainment caused by the larger filter width in *LES8*. Except for this, *LES8* simulations show similar trends of the local evaporation rate and exhibit additional tolerance in terms of *PR*. It seems that an optimal number of parcels, that provides no significant errors in the evaporation rate, should be no less than the number of physical droplets divided by the coarsen factor by which the computational cell volume was enlarged in LES from its counterpart DNS. As indicated in Table 2, $PR = 64$ in $LES4$ and $PR = 512$ in $LES8$ are the cases that closely match droplet number density of the benchmarking DNS.

To assess the Lagrangian statistics of the evaporating droplets/parcels, Figs. 6(a)–6(c) provide the Joint Probability Density Function (*JPDF*) of the normalized droplet square diameter, $d_d^2/d_{d,0}^2$, and normalized flight time, t_f/t_0 for the reference DNS and LESs with *PR=1*. In each sub-figure, the conditional averages are also reported: the mean square droplet diameter as a function of the flight time, $\langle d_d^2/d_{d,0}^2 \rangle (t/t_0)$, and the mean droplet flight time as a function of the square droplet diameter, $\langle t/t_0 \rangle (d_d^2/d_{d,0}^2)$. The statistics are directly calculated from the JPDF contours. Although the two quantities are strictly related, their meaning is different. Particularly, the mean square diameter conditioned to the flight time provides the mean square diameter of droplets given a fixed flight time, i.e., after a fixed time since droplet injection. On the other hand, the mean flight time at a given mean

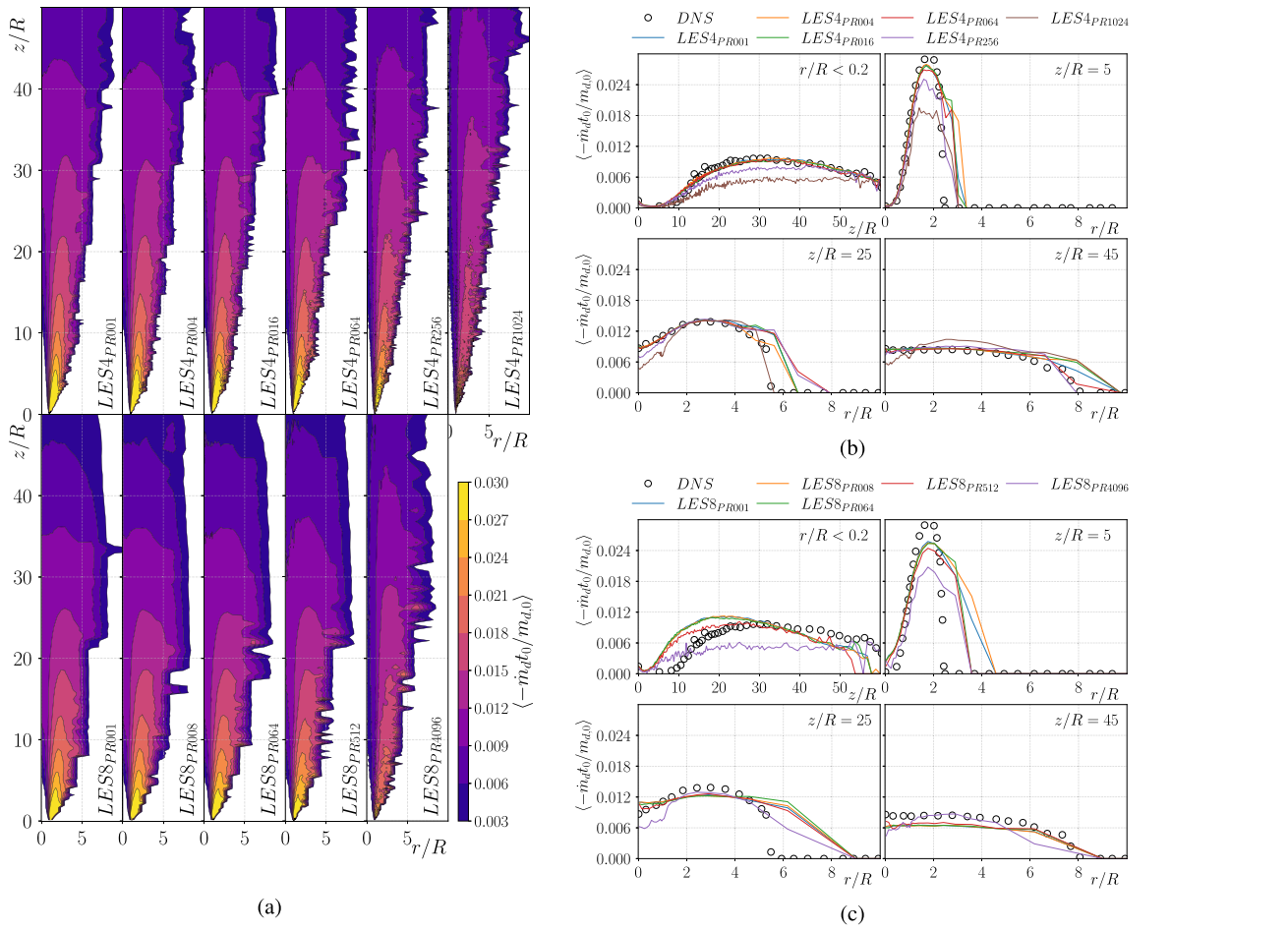

Fig. 5. (a) Mean droplet vaporization rate normalized by the reference scale defined as $\dot{m}_{d,0} = m_{d,0}/t_0$, with $m_{d,0}$ the initial droplet mass and $t_0 = R/U_0$the reference time. The results of LESs with two mesh configurations and different *PR* values are present here. Panels (b) and (c) show the distribution of the vaporization rate along the centre axis, $r/R < 0.2$, at three different z/R positions, *e.g.* z/R = 5, 25, 45. The results of the reference DNS are also included as a benchmark.

square diameter provides the amount of time needed, on average, by the droplets to reach a given size. As shown in Figs. 6(a)–6(c) LES statistics with $PR = 1$ present a generally consistent trend with the reference DNS. The two observables, in a decreasing manner, take similar values for relatively large droplets ($d_d^2/d_{d,0}^2 > 0.25$) and strongly different ones for small droplets. This suggests that the life trajectory of droplets becomes diversified mainly after losing half size of its initial diameter. The heavy-tail shape of $\langle d_d^2/d_{d,0}^2\rangle(t/t_0)$ is due to the complex dynamics coupling the droplet and the vapour concentration fields as explained in Dalla Barba and Picano (2018).

Let then consider the mean evaporation flight time, which is defined as the finite time needed, on average, by the droplets for full evaporation, t_f^e. We show the average lifetime of droplets rescaled by the advection reference time, being $t_f^e/t_0 \simeq 88$, 91 and 84 for *DNS*, *LES4* and *LES8* respectively. The *LES4*, with small deviations from DNS in terms of t_f^e/t_0, precisely replicate the average life trajectory of droplets to some extent. On the other hand the contour map and corresponding plots of *LES8* shift leftward with respect to DNS, indicating a faster evaporation process when a coarse filter is used. Since the statistical errors introduced by the grid-based estimate of average field variables are unavoidable, an appropriate filtering size needs to be selected according to the gas-phase resolution requirements.

To better quantify the influence of the parcel model on the average fate of droplets, we extract the $\langle t/t_0\rangle(d_d^2/d_{d,0}^2)$ of all cases and show their comparison in Fig. 6(d). The inset panels report the relative deviations of the average survival time of parcels in LES cases with different *PR* with respect to their counterpart LES_{PR001}. Clearly, a robust result can be achieved with *PRs* up to *64* for *LES4* and 512 for *LES8*. In this range of values, the error appears unaffected, or affected insignificantly, by the parcel ratio model. On the other hand, higher *PR* moves parcel's *destiny* rightward, indicating a longer average lifetime. In other words, with a fixed gas-phase resolution, the accuracy of the calculation will be well maintained in the range of small *PR* and deteriorate after a certain threshold. That could be attributed to the fact that when too few parcels are present in the domain, the proper non-uniform distribution of the dispersed droplets cannot be reproduced, i.e. clustering. In addition, as previously discussed, at high *PRs* the coupling source terms imposed on the carrier flow can saturate the local vapour phase in a computational cell, delaying the evaporation process. Interestingly, in the case of a higher parcel ratio in a lower accurate LES, e.g., $LES8_{PR512}$ (green dashed line), even though the whole *journey* of parcels diverges inevitably, the *destination*, t_f^e, is more proximate to that of the reference DNS compared to other *PR* values with both the filtering spacings. This implies that the error induced by the filtering method and that by parcel model may cancel each other out to some extent. We conclude that the errors become significant only after *PR* reaches a critical value. That means that if large errors are computationally acceptable on the gas-phase side, a large *PR* is also acceptable because the error will be comparable to that in the case of only physical droplets.

Unsurprisingly, the statistics presented up to now, in particular concerning the droplet vaporization characteristics, suggest a good-practice rule to perform LES with the parcel model. Note that the mesh coarsening factor for *LES4* is 64 whereas for *LES8* is 512. Thus,

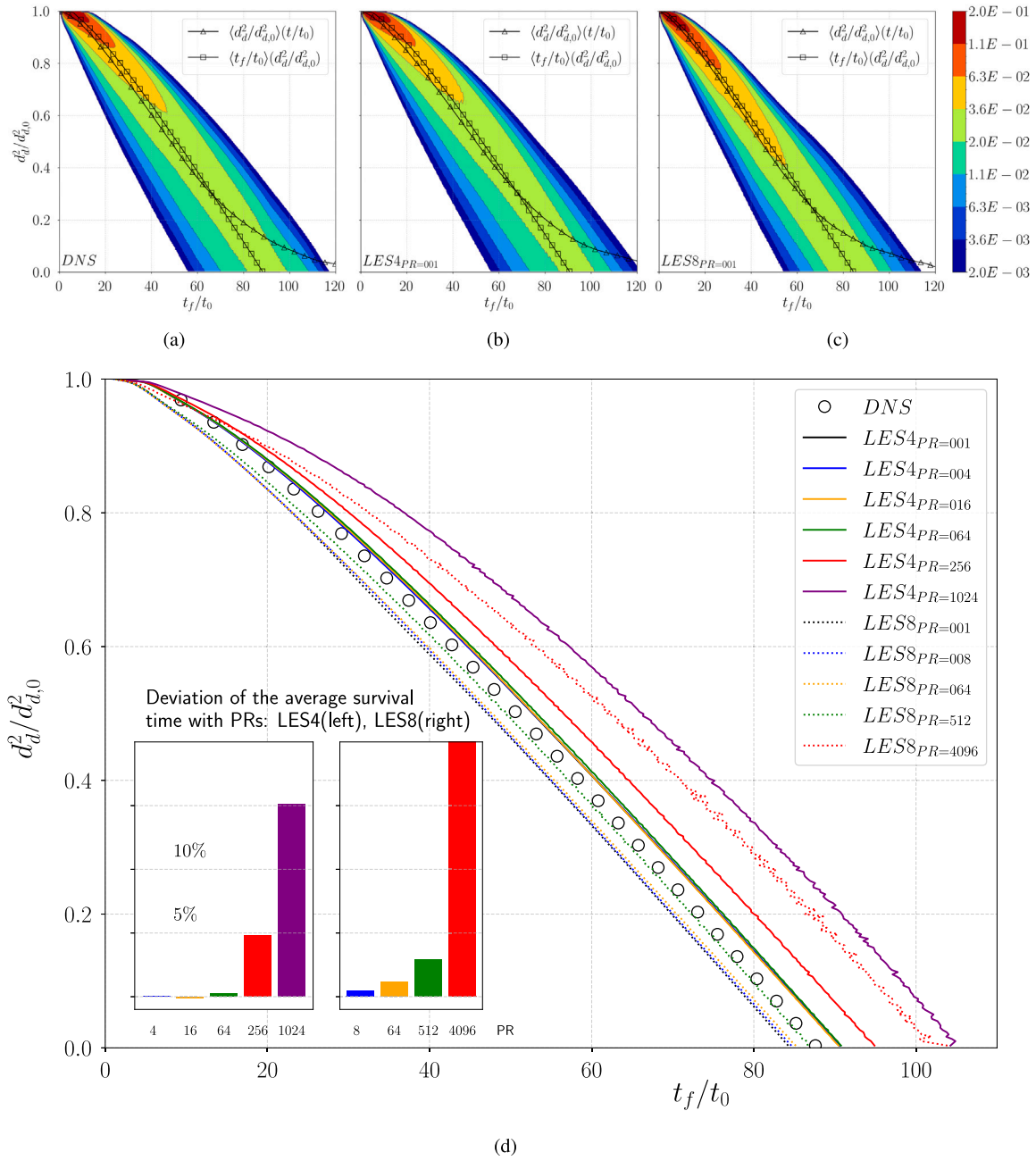

Fig. 6. (a–c) show the JPDF contour of the normalized droplet square diameter, $d_d^2/d_{d,0}^2$, and normalized flight time, t_f/t_0 for the reference DNS and LESs with bench-marking $PR = 1$. The mean square droplet diameter as a function of the flight time, $\langle d_d^2/d_{d,0}^2\rangle(t/t_0)$, and the mean droplet flight time as a function of the square droplet diameter, $\langle t/t_0\rangle(d_d^2/d_{d,0}^2)$, are also displayed for each case. (d) shows the comparisons of $\langle t/t_0\rangle(d_d^2/d_{d,0}^2)$ among all PR cases.

we believe that the best agreement with the reference DNS is indeed obtained for parcel ratios of the same order of the coarsening factor. In particular, we propose as a criterion that the parcel ratio should scale with the Eulerian degrees of freedom, and so with the coarsening extent of the Eulerian mesh size from the reference DNS to LES. This criterion can be generalized considering that the typical mesh size in DNS, Δ_{DNS}, is of the order of the dissipative length scale, η. Hence, $PR \leq \Delta_{LES}/\Delta_{DNS} \simeq PR \leq \Delta_{LES}/\eta$. In other words, in a general LES approach, the parcel ratio should be set by evaluating the ratio between the typical mesh size Δ_{LES} over the typical Kolmogorov length, η.

4. Conclusion

Even with the most modern advance in computer technology, the computational cost related to the Lagrangian tracking of droplets may be prohibitive when an enormous number of droplets need to be handled in a two-phase system. One approach to alleviate this issue is simply lowering the total number of dispersed droplets tracked in a simulation by representing a set of physical droplets having similar properties with a computational particle, the so-called *parcel*. To assess the robustness of the parcel concept, in the present work, we address the well-resolved Large-eddy Simulations (LESs) of a turbulent diluted acetone jet-spray considering different ratios of computational particles to physical droplets, i.e., parcel ratio PR.

All the thermodynamical and physical properties adopted in this study are the same as that in the reference DNS by Wang et al. (2021b), except for coarser meshes designated for the LES approach and the parcel concept. In particular, the cylindrical domain is discretized by using two coarsening factors of 4 and 8 in each direction of the corresponding

DNS mesh, while various parcel ratios are used together with a case presenting only physical droplets, namely $PR \in [1, 4, 16, 64, 256, 1024]$ for *LES4* and $[1, 8, 64, 512, 4096]$ for *LES8*. By benchmarking against LESs with only physical droplets and a reference fully resolved DNS as well, we show to which extent the parcel ratio does not cause a significant change in the statistics of the gaseous and droplet phases.

First, the numerical outcomes of the present study demonstrate the robustness of the parcel concept when the parcel ratio is carefully chosen. In particular, we show that a parcel ratio threshold exists with respect to a specific filtering-mesh configuration, and an appropriate value before this limit can provide robust statistics of droplet evaporation and dispersion in turbulent jet-sprays. Despite the statistical errors inevitably introduced by the grid-based estimate of average field variables, a significant underestimation of the mean behaviours of droplet evaporation would occur with further increases in the parcel ratio, primarily due to the inaccurate spatial distribution of parcels. Furthermore, we extrapolate a criterion that, in a general LES approach, the parcel ratio limit should be set of the same order as the ratio between the typical mesh size, Δ_{LES}, over the typical Kolmogorov length scale, η. It is worth acknowledging that this criterion is derived specifically for simulating dilute sprays under the Eulerian–Lagrangian framework with the two-way coupling method. To advance this research, it would be valuable to investigate whether the criterion remains valid for both extremely dilute and densely populated multiphase flows, using different coupling schemes. This would provide a more comprehensive understanding of the criterion's applicability across various flow conditions. We believe that the findings showed in the present study could contribute to improving the capabilities of current models in accurately and efficiently reproducing flow physics and droplet dynamics in a wide range of problems of scientific and technical interests.

CRediT authorship contribution statement

Jietuo Wang: Conceptualization, Methodology, Software, Validation, Formal analysis, Investigation, Data curation, Writing – original draft, Writing – review & editing, Visualization. **Federico Dalla Barba:** Conceptualization, Methodology, Investigation, Data curation, Writing – review & editing.

Declaration of competing interest

The authors declare that they have no known competing financial interests or personal relationships that could have appeared to influence the work reported in this paper.

Data availability

Data will be made available on request.

Acknowledgments

This work was supported by China Scholarship Council (CSC) Grant #201806250023.

References

Abramzon, B., Sirignano, William A., 1989. Droplet vaporization model for spray combustion calculations. Int. J. Heat Mass Transfer 32 (9), 1605–1618.
Alobaid, F., 2015. A particle–grid method for Euler–Lagrange approach. Powder Technol. 286, 342–360.
Amsden, Anthony A., O'Rourke, Peter J., Butler, T. Daniel, 1989. KIVA-II: A computer program for chemically reactive flows with sprays. Technical report, Los Alamos National Lab.(LANL), Los Alamos, NM (United States).
Apte, S.V., Gorokhovski, Mikhael, Moin, Parviz, 2003. LES of atomizing spray with stochastic modeling of secondary breakup. Int. J. Multiph. Flow. 29 (9), 1503–1522.
Apte, Sourabh V, Mahesh, Krishnan, Gorokhovski, Michael, Moin, Parviz, 2009. Stochastic modeling of atomizing spray in a complex swirl injector using large eddy simulation. Proc. Combust. Inst. 32 (2), 2257–2266.
Ardekani, Mehdi Niazi, Costa, Pedro, Breugem, Wim Paul, Brandt, Luca, 2016. Numerical study of the sedimentation of spheroidal particles. Int. J. Multiph. Flow. 87, 16–34.
Balachandar, S., 2009. A scaling analysis for point–particle approaches to turbulent multiphase flows. Int. J. Multiph. Flow. 35 (9), 801–810.
Balachandar, S., Eaton, John K., 2010. Turbulent dispersed multiphase flow. Annu. Rev. Fluid Mech. 42, 111–133.
Balachandar, S., Liu, Kai, Lakhote, Mandar, 2019. Self-induced velocity correction for improved drag estimation in Euler–Lagrange point-particle simulations. J. Comput. Phys. 376, 160–185.
Brandt, Luca, Coletti, Filippo, 2021. Particle-laden turbulence: Progress and perspectives. Annu. Rev. Fluid Mech. 54.
Burton, Tristan M., Eaton, John K., 2005. Fully resolved simulations of particle-turbulence interaction. J. Fluid Mech. 545, 67–111.
Chen, Yung-Cheng, Stårner, Sten H., Masri, Assaad R., 2006. A detailed experimental investigation of well-defined, turbulent evaporating spray jets of acetone. Int. J. Multiph. Flow. 32 (4), 389–412.
Ciottoli, Pietro P, Battista, F, Malpica Galassi, R, Dalla Barba, F, Picano, F, 2021. Direct numerical simulations of the evaporation of dilute sprays in turbulent swirling jets. Flow Turbul. Combust. 106, 993–1015.
Dalla Barba, Federico, 2016. High performance computing of turbulent evaporating sprays Master's thesis. University of Padova.
Dalla Barba, Federico, Picano, Francesco, 2018. Clustering and entrainment effects on the evaporation of dilute droplets in a turbulent jet. Phys. Rev. Fluids 3 (3), 034304.
Druzhinin, O.A., Elghobashi, S., 1998. Direct numerical simulations of bubble-laden turbulent flows using the two-fluid formulation. Phys. Fluids 10 (3), 685–697.
Dukowicz, John K., 1980. A particle-fluid numerical model for liquid sprays. J. Comput. Phys. 35 (2), 229–253.
Elghobashi, Said, 1994. On predicting particle-laden turbulent flows. Appl. Sci. Res. 52, 309–329.
Favre, Alexandre, 1983. Turbulence: Space-time statistical properties and behavior in supersonic flows. Phys. Fluids 26 (10), 2851–2863.
Fox, Rodney O., Laurent, Frédérique, Massot, Marc, 2008. Numerical simulation of spray coalescence in an Eulerian framework: direct quadrature method of moments and multi-fluid method. J. Comput. Phys. 227 (6), 3058–3088.
Froessling, Nils, 1968. On the evaporation of falling drops. Technical report, ARMY BIOLOGICAL LABS FREDERICK MD.
Garg, R., Narayanan, C., Subramaniam, S., 2009. A numerically convergent Lagrangian–Eulerian simulation method for dispersed two-phase flows. Int. J. Multiph. Flow. 35 (4), 376–388.
Gualtieri, Paolo, Picano, F, Sardina, Gaetano, Casciola, Carlo Massimo, 2015. Exact regularized point particle method for multiphase flows in the two-way coupling regime. J. Fluid Mech. 773, 520–561.
Horwitz, J.A.K., Mani, A., 2018. Correction scheme for point-particle models applied to a nonlinear drag law in simulations of particle-fluid interaction. Int. J. Multiph. Flow. 101, 74–84.
Johnson, Perry L., 2020. Predicting the impact of particle-particle collisions on turbophoresis with a reduced number of computational particles. Int. J. Multiph. Flow. 124, 103182.
Lau, Timothy C.W., Nathan, Graham J., 2014. Influence of Stokes number on the velocity and concentration distributions in particle-laden jets. J. Fluid Mech. 757, 432–457.
Lau, Timothy C.W., Nathan, Graham J., 2016. The effect of Stokes number on particle velocity and concentration distributions in a well-characterised, turbulent, co-flowing two-phase jet. J. Fluid Mech. 809, 72–110.
Marchioli, Cristian, 2017. Large-eddy simulation of turbulent dispersed flows: a review of modelling approaches. Acta Mech. 228 (3), 741–771.
Maxey, Martin R., Riley, James J., 1983. Equation of motion for a small rigid sphere in a nonuniform flow. Phys. Fluids 26 (4), 883–889.
Mostafa, A.A., Mongia, H.C., 1987. On the modeling of turbulent evaporating sprays: Eulerian versus Lagrangian approach. Int. J. Heat Mass Transfer 30 (12), 2583–2593.
Okong'o, Nora A., Bellan, Josette, 2004. Consistent large-eddy simulation of a temporal mixing layer laden with evaporating drops. Part 1. Direct numerical simulation, formulation and a priori analysis. J. Fluid Mech. 499, 1–47.
Patankar, N.A., Joseph, D.D., 2001. Modeling and numerical simulation of particulate flows by the Eulerian–Lagrangian approach. Int. J. Multiph. Flow. 27 (10), 1659–1684.
Picano, F., Sardina, G., Gualtieri, P., Casciola, C.M., 2010. Anomalous memory effects on transport of inertial particles in turbulent jets. Phys. Fluids 22 (5), 051705.
Radhakrishnan, Senthilkumaran, Bellan, Josette, 2012. Influence of computational drop representation in LES of a mixing layer with evaporating drops. Comput. & Fluids 58, 15–26.
Rocco, Gabriele, Battista, Francesco, Picano, Francesco, Troiani, Guido, Casciola, Carlo Massimo, 2015. Curvature effects in turbulent premixed flames of h 2/air: a DNS study with reduced chemistry. Flow Turbul. Combust. 94, 359–379.
Salewski, Mirko, 2006. LES of Jets and Sprays Injected Into Crossflow. Lund University.
Sankaran, Vaidyanathan, Menon, Suresh, 2002. LES of spray combustion in swirling flows. J. Turbul. 3 (1), 011.

Schmidt, Helmut, Schumann, Ulrich, 1989. Coherent structure of the convective boundary layer derived from large-eddy simulations. J. Fluid Mech. 200, 511–562.
Smagorinsky, Joseph, 1963. General circulation experiments with the primitive equations: I. The basic experiment. Mon. Weather Rev. 91 (3), 99–164.
Spalding, Dudley Brian, 1950. Combustion of liquid fuels. Nature 165 (4187), 160.
Squires, Kyle D., Eaton, John K., 1990. Particle response and turbulence modification in isotropic turbulence. Phys. Fluids A: Fluid Dyn. 2 (7), 1191–1203.
Subramaniam, Shankar, 2013. Lagrangian–Eulerian methods for multiphase flows. Prog. Energy Combust. Sci. 39 (2–3), 215–245.
Wang, Jietuo, 2022. Simulation and modelling turbulent spray dynamics (Ph.D. thesis). University of Padova.
Wang, Jietuo, Alipour, Mobin, Soligo, Giovanni, Roccon, Alessio, De Paoli, Marco, Picano, Francesco, Soldati, Alfredo, 2021a. Short-range exposure to airborne virus transmission and current guidelines. Proc. Natl. Acad. Sci. USA 118 (37), e2105279118.
Wang, Jietuo, Dalla Barba, Federico, Picano, Francesco, 2021b. Direct numerical simulation of an evaporating turbulent diluted jet-spray at moderate Reynolds number. Int. J. Multiph. Flow. 137, 103567.